Influence of sulfation on iron titanate catalyst for the selective catalytic reduction of NO$_x$ with NH$_3$

Fudong Liu[a], Kiyotaka Asakura[b], Hong He[a,*], Wenpo Shan[a], Xiaoyan Shi[a], Changbin Zhang[a]

[a] State Key Laboratory of Environmental Chemistry and Ecotoxicology, Research Center for Eco-Environmental Sciences, Chinese Academy of Sciences, Beijing 100085, PR China
[b] Catalysis Research Center, Hokkaido University, Sapporo 001-0021, Japan

ARTICLE INFO

ABSTRACT

Iron titanate catalyst (FeTiO$_x$) is a potential candidate for the substitution of conventional V$_2$O$_5$–WO$_3$ (MoO$_3$)/TiO$_2$ and Fe/Cu-zeolite catalysts for the selective catalytic reduction (SCR) of NO$_x$ with NH$_3$ because of its high SCR activity and N$_2$ selectivity in the medium temperature range. Due to the presence of small amount of SO$_2$ in typical diesel exhaust derived from combustion of sulfur-containing fuels, it is very important to investigate the influence of sulfation on SCR activity, catalyst structure and reaction mechanism. After sulfation under the SCR condition, the surface area and pore volume of FeTiO$_x$ catalyst decreased to a certain extent due to the formation of sulfate species. According to the characterizations of FeTiO$_x$ catalyst using X-ray diffraction, X-ray absorption fine structure spectroscopy, and *in situ* diffuse reflectance infrared Fourier transform spectroscopy of SO$_2$ + O$_2$ treatment, the sulfate species mainly formed on iron sites in a chelating bidentate conformation, resulting in the enhancement of Brønsted acidity and Lewis acid strength simultaneously. NH$_3$ adsorption was greatly enhanced in the high temperature range, while NO$_x$ adsorption was severely inhibited due to the stronger acidity of sulfate species. The operation temperature window of the sulfated catalyst shifted *ca.* 50 °C towards high temperature range accordingly. The reaction mechanism study shows that the Langmuir–Hinshelwood reaction pathway was cut off by the sulfation process, resulting in the activity loss at low temperatures; only Eley–Rideal reaction pathway between adsorbed NH$_3$ species and gaseous or weakly adsorbed NO dominated in the SCR reaction, which made this catalyst resistant to SO$_2$ poisoning at relatively high temperatures.

© 2011 Elsevier B.V. All rights reserved.

1. Introduction

Selective catalytic reduction (SCR) of NO$_x$ with NH$_3$ over V$_2$O$_5$–WO$_3$ (MoO$_3$)/TiO$_2$ catalyst is a well proven technique for the removal of NO$_x$ from stationary and mobile sources [1]. Due to some inevitable disadvantages of the present vanadium-based catalyst including the narrow operation temperature window and the toxicity of vanadium pentoxide *etc.* [2,3], more and more researchers are focusing on the development of new vanadium-free SCR catalysts, such as Fe-, Cu-, Mn-, Ce-based exchanged zeolites, supported type or mixed oxide catalysts [3–14]. In our previous study, we also reported a novel and environmental-friendly iron titanate catalyst (FeTiO$_x$) prepared by facile co-precipitation method showing excellent SCR activity and N$_2$ selectivity in medium temperature range, which is possibly suitable for the DeNO$_x$ process for diesel engines [15–17]. It is well known that nowadays the typical diesel

exhaust usually contains a small amount of SO$_2$ below 50 ppm from the combustion of sulfur-containing fuels. Even when using fuels and engine oils with "ultra low" sulfur content (<15 ppm) in the near future, the exhaust after combustion in lean burn conditions still contains some fractions of SO$_2$ [18]. After long time SCR reaction, even this small amount of SO$_2$ can deactivate the SCR catalysts due to the formation of metal sulfate species, the blockage of catalyst pore channels or the cutting off of redox cycle of active phases [14,19,20]. So far as known, no vanadium-free catalyst can exhibit both high SCR activity and high SO$_2$ durability at the same time below 200 °C. Additionally, the SCR reaction mechanism over sulfated catalyst may also differ from that over the fresh one. It is important, therefore, to investigate the influence of sulfation on the activity and structure of our FeTiO$_x$ catalyst, which will help understand the deactivation mechanism and further improve of its SO$_2$ durability in future studies.

In our previous study, we have already investigated the SO$_2$ durability (100 ppm) of FeTiO$_x$ catalyst in the SCR reaction at a fixed temperature (300 °C), with no obvious decrease of NO conversion observed in a 48 h test [15]. In this study, the influence of sulfation on this catalyst in a wider temperature range (150–400 °C) will be

---

* Corresponding author at: P.O. Box 2871, 18 Shuangqing Road, Haidian District, Beijing 100085, PR China. Tel.: +86 10 62849123; fax: +86 10 62849123.
  E-mail address: honghe@rcees.ac.cn (H. He).

studied. More specifically, the SCR activity over $FeTiO_x$ catalysts before and after sulfation will be tested using steady-state reaction and temperature programmed surface reaction (TPSR), which are more comprehensive for the activity evaluation. In addition, we will fully investigate the influence of sulfation in SCR condition on catalyst structure using N_2 physisorption, X-ray diffraction (XRD), X-ray absorption fine structure spectroscopy (XAFS), and X-ray photo-electron spectroscopy (XPS). The sulfation sites on this catalyst will also be discussed in detail. Over pre-sulfated catalyst, temperature programmed desorption of NH_3 and NO_x (NH_3/NO_x-TPD) together with *in situ* diffuse reflectance infrared Fourier transform spectroscopy (*in situ* DRIFTS) will be used to elucidate the change of SCR reaction mechanism comparing with that over the fresh catalyst.

2. Experimental

2.1. Catalyst preparation

Iron titanate catalyst ($FeTiO_x$-fresh) using $Fe(NO_3)\cdot 9H_2O$ and $Ti(SO_4)_2$ (Fe:Ti = 1:1 in molar ratio) as precursors was calcined at 400 °C for 6 h before use. Other preparation procedures have been described in detail in our previous studies [15,16]. In the present study, sulfated $FeTiO_x$ catalysts were obtained by pretreating $FeTiO_x$-fresh in a flow of 500 ppm NH_3 + 500 ppm NO + 5 vol.% O_2 + 100 ppm SO_2 (SCR condition) or 100 ppm SO_2 + 5 vol.% O_2 at 300 °C for 48 h. The former sample was denoted as "$FeTiO_x$-sulfation in SCR" for steady-state SCR activity test and characterizations, and the latter one was denoted as "$FeTiO_x$-sulfation" for TPSR experiments and reaction mechanism study.

2.2. Activity test

The steady-state SCR activity over $FeTiO_x$ catalysts before and after sulfation in SCR condition was performed in a fixed-bed quartz tube reactor. The reaction conditions were controlled as follows: 0.6 ml catalysts, 500 ppm NO, 500 ppm NH_3, 5 vol.% O_2, N_2 balance and gas hourly space velocity (GHSV) of 50,000 h^{-1}. The effluent gas was continuously analyzed using an FTIR spectrometer (Nicolet Nexus 670) equipped with a heated, low volume multiple-path gas cell (2 m). The TPSR experiments in SCR condition were performed over fresh and pre-sulfated $FeTiO_x$ catalysts (100 mg) using a quadrupole mass spectrometer (HPR20, Hiden Analytical Ltd.) to record the signal of NO (m/z = 30). The samples were firstly pretreated at 300 °C for 0.5 h in a flow of 20 vol.% O_2/He (30 ml/min) and cooled down to room temperature. The samples were then exposed to a flow of 500 ppm NH_3 + 500 ppm NO + 5 vol.% O_2 (30 ml/min) for 1 h until the signals of mass spectrometer were stabilized. Finally, the temperature was raised linearly to 500 °C at the rate of 10 °C/min in the same gas flow.

2.3. Characterizations

The N_2 adsorption–desorption isotherms were obtained at −196 °C using a Quantachrome Autosorb-1C instrument. Prior to N_2 physisorption, the catalysts were degassed at 300 °C for 4 h. Surface areas were determined by BET equation in 0.05–0.35 partial pressure range. Pore volumes and average pore diameters were determined by Barrett–Joyner–Halenda (BJH) method from desorption branches of the isotherms.

The XRD measurements were conducted on a Rigaku D/max-RB Diffractometer (Japan, Cu K_α as radiation resource). The data of 2θ from 10 to 90° were collected at 4°/min with the step size of 0.02°.

The XAFS spectra of Fe, Ti K-edges and S K-edge were recorded at room temperature in a transmission mode on BL-7C beam line and in a fluorescence mode on BL-9A beam line, respectively, at Photon Factory, Institute of Materials Structure Science (IMSS-KEK), Japan.

The storage ring was operated at 2.5 GeV with an average storage current of 300 mA. The synchrotron radiation was monochromatized with a Si (1 1 1) double crystal monochromator, and mirrors were used to eliminate higher harmonics. The incident and transmitted beam intensities were monitored using ionization chambers filled with pure N_2. For the XAFS measurement of S K-edge, the entire beam path was filled with He to suppress the X-ray absorption and scattering by air. Data were analyzed using the REX2000 program (Rigaku Co.). The EXAFS (extended X-ray absorption fine structure) oscillations $\chi(k)$ of Fe and Ti K-edges were extracted using spline smoothing with a Cook–Sayers criterion [21], and the filtered k^3-weighted $\chi(k)$ was Fourier transformed into R space (k range: 2.5–15 Å^{-1} for Fe K-edge EXAFS and 2.5–13 Å^{-1} for Ti K-edge EXAFS). In the curve fitting step, the backscattering amplitude and phase shift were calculated using FEFF8.4 [22]. The XANES (X-ray absorption near edge structure) of S K-edge were normalized by the edge height and then the first-order derivatives were determined to compare the variation of absorption edge energies.

The XPS were recorded on a Scanning X-ray Microprobe (PHI Quantera, ULVAC-PHI, Inc.) using Al K_α radiation. Binding energies of S 2p, O 1s, Fe 2p and Ti 2p were calibrated using C 1s peak (BE = 284.8 eV) as standard.

2.4. Reaction mechanism study

NH_3-TPD and NO_x-TPD experiments were performed on 100 mg samples using the above-mentioned quadrupole mass spectrometer to record the signals of NH_3 (m/z = 16) and NO_x (m/z = 30). Prior to the TPD procedure, the samples were pretreated at 300 °C for 0.5 h in a flow of 20 vol.% O_2/He (30 ml/min) and cooled down to room temperature. The samples were then exposed to a flow of 2500 ppm NH_3/Ar or 2500 ppm NO + 10 vol.% O_2/Ar (30 ml/min) for 1 h, followed by Ar purge for another 1 h. Finally, the temperature was raised to 500 °C in Ar flow at the rate of 10 °C/min.

The *in situ* DRIFTS experiments were performed on an FTIR spectrometer (Nicolet Nexus 670) equipped with a smart collector and an MCT/A detector cooled by liquid nitrogen. The reaction temperature was controlled precisely by an Omega programmable temperature controller. Prior to each experiment, the sample was pretreated at 400 °C for 0.5 h in a flow of 20 vol.% O_2/N_2 and then cooled down to the desired temperature. The background spectrum was collected in flowing N_2 and automatically subtracted from the sample spectrum. The reaction conditions were controlled as follows: 300 ml/min total flow rate, 500 ppm NH_3, 500 ppm NO, 500 ppm SO_2 (when used for SO_2 + O_2 treatment experiments), 5 vol.% O_2 and N_2 balance. All spectra were recorded by accumulating 100 scans with a resolution of 4 cm^{-1}. In order not to lose any structural or surface information in DRIFTS study, the background spectra of Fe_2O_3, TiO_2, $FeTiO_x$-fresh and $FeTiO_x$-sulfation are also presented in Fig. S1, which indicate that in the preparation process a small amount of sulfate derived from $Ti(SO_4)_2$ precursor was already present on the surface of TiO_2 and $FeTiO_x$-fresh. The further sulfation of $FeTiO_x$ catalyst resulted in the deposition of more sulfate species on the catalyst surface, which can be clearly seen from the broadening and the blue shift of corresponding IR band.

3. Results and discussion

3.1. SCR activity

The SCR activity over $FeTiO_x$ catalysts before and after sulfation was tested using steady-state reaction and TPSR methods, and the results are shown in Fig. 1. After sulfation, the steady-state SCR activity showed an obvious decrease below 250 °C and some increase above 350 °C. In the TPSR experiments in a flow of
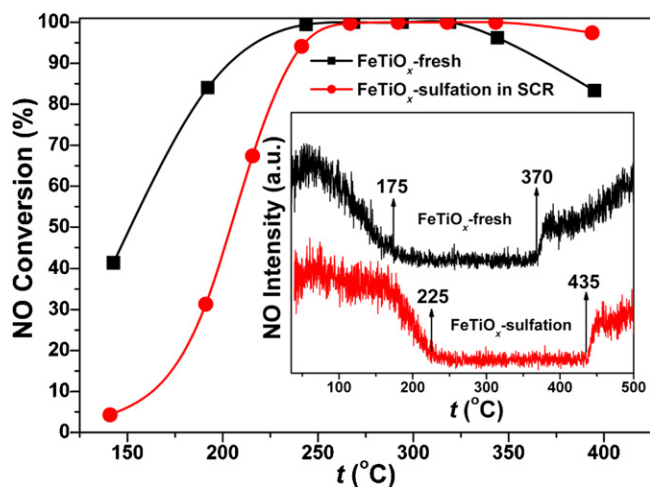
Fig. 1. SCR activity over $FeTiO_x$ catalysts before and after sulfation (inset: TPSR in a flow of $NH_3 + NO + O_2$).

Fig. 2. XRD results of $FeTiO_x$-fresh and $FeTiO_x$-sulfation in SCR together with standard cards of $Fe_2(SO_4)_3$ and $Ti(SO_4)_2$ in JCPDS.

$NH_3 + NO + O_2$, as shown in the inset figure, the NO concentration over both $FeTiO_x$-fresh and $FeTiO_x$-sulfation showed an obvious decrease with the increasing of reaction temperature, implying the occurrence of the SCR reaction. The decline of NO concentration over $FeTiO_x$-sulfation started at much higher temperature (*ca.* 150 °C) than that over $FeTiO_x$-fresh (<100 °C), indicating the loss of low temperature activity over sulfated catalyst. Accordingly, the highest NO conversion over $FeTiO_x$-sulfation was obtained in a temperature window of 225–435 °C, which was 50 °C delayed comparing with that over $FeTiO_x$-fresh (175–370 °C). At relatively high temperatures, the unselective oxidation of NH_3 occurred, resulting in the increase of NO concentration. The sulfation suppressed this unselective oxidation side-reaction to a certain extent, and the operation temperature window over $FeTiO_x$-sulfation was slightly enlarged accordingly. It is noteworthy that the temperature points achieving maximum NO conversions over $FeTiO_x$ catalysts before and after sulfation in TPSR experiments were relatively lower than those in the steady-state SCR activity tests. This is probably because the NH_3 adsorption/desorption was not fast enough in transient-state when the temperature ramp rate was kept at 10 °C/min, resulting in the presence of more NH_3 adsorbed species than that in steady-state at low temperatures.

3.2. N₂ physisorption

Table 1 shows the structural parameters of $FeTiO_x$ catalysts before and after sulfation derived from N_2 physisorption results. After sulfation in the SCR condition, the BET surface area of $FeTiO_x$ catalyst decreased from 245.3 to 213.5 m^2/g, and the BJH cumulative desorption pore volume also decreased from 0.52 to 0.40 cm^3/g. This may have led to the SCR activity loss over the sulfated catalyst. As we can see, the fresh catalyst was mainly composed of mesopores with an average pore diameter of 8.3 nm. After sulfation, the average pore diameter showed a decrease to 7.4 nm, indicating the forma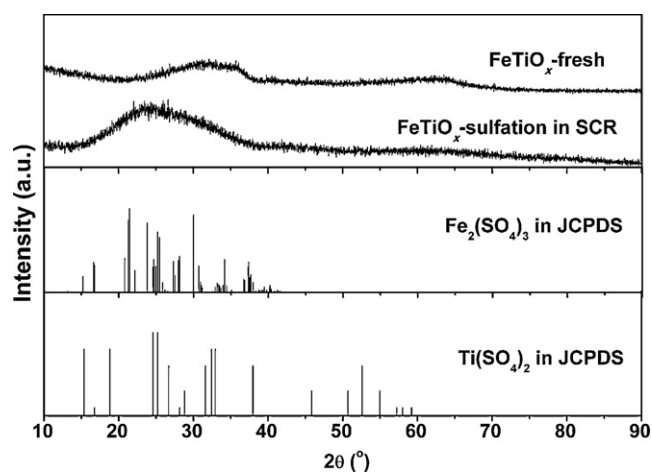tion of some smaller pores due to the deposition of sulfate species. The sulfate species produced in this process could be ammonium sulfate/bisulfate resulting from gaseous reactants or metal sulfates because of the reaction between SO_2 and $FeTiO_x$ catalyst, such as ferric sulfate or titanic sulfate. The formed sulfate species and the sulfation sites of $FeTiO_x$ catalyst will be discussed in detail in following sections.

3.3. XRD

Fig. 2 shows the comparative XRD results of $FeTiO_x$-fresh and $FeTiO_x$-sulfation in SCR together with the standard cards of $Fe_2(SO_4)_3$ and $Ti(SO_4)_2$ in JCPDS. In our previous study [15,16], we have concluded that the $FeTiO_x$-fresh catalyst was mainly in the form of iron titanate crystallites (Fe_2TiO_5 or $FeTiO_3$), which displayed large broad bumps at the positions as shown in Fig. 2. After sulfation, the $FeTiO_x$ catalyst was still not well-crystallized, showing no obvious diffraction peaks. However, another broad bump appeared at a different position, implying the formation of another crystallite species. Compared to the standard cards of $Fe_2(SO_4)_3$ and $Ti(SO_4)_2$ in JCPDS, we can deduce that this crystallite species was mainly composed of ferric sulfate, because no diffraction signals were observed at 15.4 and 52.6° where $Ti(SO_4)_2$ should exhibit distinct diffraction peaks. The sulfate species favored to form on iron sites than on titanium sites at the sulfation temperature that we set, because ferric sulfate is more thermodynamically stable and usually decomposes above 480 °C [23], whereas titanic sulfate cannot form in SO_2-containing atmosphere above 200 °C [24]. In addition, the formation of ammonium sulfate/bisulfate particles cannot be excluded according to the XRD results because these species also showed typical diffraction peaks between 20 and 30°. Previous research has indicated that at around 280 °C pure ammonium sulfate can decompose into ammonium bisulfate [25], which was more stable up to 390 °C (for pure NH_4HSO_4) [26]. However, on some catalyst surface the decomposing temperature of these species can be further lowered, such as 250 °C for NH_4HSO_4 over V_2O_5/AC [26]. Therefore, even if these sulfate species could deposit on the surface of $FeTiO_x$ catalyst, the amount should be rather small and neglectable because the sulfation temperature in this study was set at 300 °C. The formation of ammonium sulfate/bisulfate particles leading to the blockage of some pore channels should not be the main reason for the catalyst deactivation. The structure change of iron sites after sulfation in this catalyst should be critical for the variation of catalytic performance, which can be proved by the subsequent experimental results.

Table 1
Structural parameters of $FeTiO_x$ catalysts before and after sulfation derived from N_2 physisorption results.

Samples	S_{BET} (m^2/g)[a]	Pore volume (cm^3/g)[b]	Pore diameter (nm)[c]
$FeTiO_x$-fresh	245.3	0.52	8.3
$FeTiO_x$-sulfation in SCR	213.5	0.40	7.4

[a] BET surface area.
[b] BJH desorption pore volume.
[c] Average pore diameter.

3.4. XAFS

Fig. 3A and B shows the EXAFS oscillations $k^3 \cdot \chi(k)$ and corresponding Fourier transforms of filtered $k^3 \cdot \chi(k)$ into R space of Fe K-edge in $Fe_2(SO_4)_3$ reference sample and $FeTiO_x$ catalysts before and after sulfation. New EXAFS oscillations of Fe K-edge in $FeTiO_x$ catalyst occurred after sulfation at some k values, as the dashed arrows shown in Fig. 3A, which may be attributed to Fe–O–S oscillations. As shown in Fig. 3B, for the $FeTiO_x$-fresh catalyst, the first peak in R space was attributed to Fe–O bond in the first coordination shell and the second peak to Fe–O–Ti bond in the second coordination shell [16]. For the $Fe_2(SO_4)_3$ reference sample, the first peak was also attributed to Fe–O bond but with larger bond distance than that in $FeTiO_x$, and the second peak was attributed to Fe–O–S bond also with larger bond distance than that of Fe–O–Ti. As we can see, after sulfation the Fe–O bond distance in $FeTiO_x$ catalyst showed some increase. At the same time, another shoulder peak appeared at a longer distance than that of Fe–O–Ti bond, indicating the formation of some Fe–O–S structure. Comparatively, the EXAFS oscillations $k^3 \cdot \chi(k)$ and corresponding Fourier transforms of filtered $k^3 \cdot \chi(k)$ into R space of Ti K-edge in the $Ti(SO_4)_2$ reference sample and $FeTiO_x$ catalysts before and after sulfation are shown in Fig. 3C and D. Obviously, no change was observed for EXAFS oscillations of Ti K-edge in $FeTiO_x$ catalyst after sulfation. Accordingly, both Ti–O and Ti–O–Fe bonds in R space also showed no obvious variation after sulfation, and no new peak attributed to $Ti(SO_4)_2$ species appeared. These results imply that sulfate species was mainly formed on iron sites, but not titanium sites of $FeTiO_x$ catalyst during the sulfation process. To further confirm the state of the formed sulfate species, S K-edge XANES spectra of $Fe_2(SO_4)_3$, $Ti(SO_4)_2$ and $FeTiO_x$ catalyst after sulfation are presented in Fig. 3E. Not only the pre-edge peak intensity but also the absorption edge energy (see first-order derivatives in the inset figure) of S K-edge in $FeTiO_x$ after sulfation were identical to those of $Fe_2(SO_4)_3$, implying again the formation of sulfate species on iron sites. Fig. 3F shows the difference between the spectra of Fe K-edge EXAFS oscillations in $FeTiO_x$ catalysts before and after sulfation, with the red dots corresponding to the calculated EXAFS oscillations of Fe–O–S bond in $Fe_2(SO_4)_3$ using FEFF. Good curve fitting results were obtained as shown by the fitting data in Table 2, validating the formation of Fe–O–S structure again. The validity of the FEFF calculated phase shift and amplitude function are also confirmed by the curve fitting result of the second coordination shell in $Fe_2(SO_4)_3$ reference sample using Fe–O–S scattering path (as shown in Fig. S2), which are in good accordance with the crystallographic data within 0.01 Å.

3.5. XPS

The oxidation states of surface elements on $FeTiO_x$ catalysts before and after sulfation in the SCR condition were characterized using XPS, as the results shown in Fig. 4. On the $FeTiO_x$-fresh catalyst, no obvious S 2p band was observed in Fig. 4A, and the S content was calculated to be only 0.2% in molar ratio, which was resulted from residual sulfate species from the $Ti(SO_4)_2$ precursor. After sulfation, an evident band attributed to S 2p was observed and the S content also increased to 4.7%, implying the formation of sulfur-containing species on the catalyst surface. The binding energy of this S 2p band was 169.1 eV, which was typical for S^{6+} in the form of SO_4^{2-} connecting to the iron sites according to the XRD and XAFS results [27–30]. The O 1s bands in Fig. 4B were deconvoluted by searching for the optimal combination of Gaussian sub-bands with the correlation coefficients (r^2) above 0.99 (PeakFit software package, Version 4.12, SeaSolve Software Inc.). The sub-bands at lower binding energy (530.2–530.5 eV) corresponded to the lattice oxygen O^{2-} (denoted as O_β), and the sub-bands at higher binding energy (531.6–532.1 eV) corresponded to the surface adsorbed oxygen (denoted as O_α), such as O_2^{2-} or O^- belonging to defect-oxide or hydroxyl-like group [31]. After sulfation, both of the O_α and O_β bands shifted towards higher binding energies (0.3–0.5 eV) due to the stronger electron affinity by S^{6+} in SO_4^{2-}. In addition, the ratio of $O_\alpha/(O_\alpha + O_\beta)$ increased from 28% to 51% after sulfation, indicating the presence of more hydroxyls on the catalyst surface. We inferred that these surface hydroxyls were mainly acidic due to the hydration of SO_4^{2-} to form S–OH group, supplying more Brønsted acid sites to adsorb NH_3 in the form of NH_4^+ during the SCR process. This hypothesis can be verified by the following *in situ* DRIFTS experiments.

The XPS results of Fe 2p and Ti 2p are shown in Fig. 4C and D, respectively. On the $FeTiO_x$-fresh catalyst, the binding energies of Fe $2p_{3/2}$ (711.1 eV) and Fe $2p_{1/2}$ (724.9 eV) corresponded well with those of Fe^{3+}, and the binding energies of Ti $2p_{3/2}$ (458.6 eV) and Ti $2p_{1/2}$ (464.3 eV) were typical characteristics of Ti^{4+} [32,33]. After sulfation in the SCR condition, both of the Fe 2p and Ti 2p bands shifted towards higher binding energies (*ca.* 0.5 eV). This was mainly due to the inductive effect of the S=O covalent double bond with a much stronger affinity to electrons [34,35], implying an enhanced Lewis acid strength of metallic sites on the catalyst surface. This inductive effect also resulted in the enhanced Brønsted acidity when H_2O molecules adsorbed on unsaturated metallic sites to form surface acidic hydroxyls [34,36]. Therefore, together with the extra Brønsted acid sites introduced by sulfate species itself, the surface Brønsted acidity and Lewis acid strength derived from metallic sites on $FeTiO_x$ catalyst were also simultaneously improved by the sulfation process. On one hand, this will provide more acid sites for the adsorption of NH_3, supplying more reducing agent for the SCR reaction especially in the relatively high temperature range. On the other hand, however, too strong affinity of NH_3 by the sulfated catalyst in the relatively low temperature range would inhibit the NH_3 activation and then decrease the low temperature SCR activity to a certain extent.

3.6. In situ DRIFTS of $SO_2 + O_2$ treatment

To further elucidate the surface sulfate species and the sulfation sites on $FeTiO_x$ catalyst, *in situ* DRIFTS of $SO_2 + O_2$ treatment on Fe_2O_3, $FeTiO_x$-fresh and TiO_2 were carried out at 200 °C and the results are shown in Fig. 5. As shown in Fig. 5A, obvious overlapped vibration bands appeared from 800 to 1400 cm^{-1} in the spectrum of Fe_2O_3 after sulfation, which were generally attributed to sulfur-containing species. Several sharp negative bands at 3631, 3666 and 3724 cm^{-1} were observed, indicating the consumption of surface basic hydroxyls through interaction with SO_2 [37]. An obvious band at 1614 cm^{-1} ascribed to δ_{HOH} vibration mode also appeared, implying the formation of H_2O in the sulfation process or the adsorption of trace of H_2O from simulating gas [38,39]. The presence of a large broad band in the range of 3000–3500 cm^{-1} due to the O–H stretching vibration mode also confirmed this point of view [38]. As for the $FeTiO_x$ catalyst after $SO_2 + O_2$ treatment for the same time, similar bands as those observed on Fe_2O_3 appeared, including overlapped bands of sulfur-containing species in the range of 900–1400 cm^{-1}, hydroxyl consumption bands at 3724 and 3691 cm^{-1} together with the H_2O adsorption band at 1614 cm^{-1}. The major difference was that the intensity of these bands was much lower than those on Fe_2O_3, indicating that less amount of sulfur-containing species was formed on the catalyst surface. The presence of titanium species in the $FeTiO_x$ catalyst could hinder the sulfation process to a certain extent, weakening the SO_2 poisoning effect in the SCR reaction. The TiO_2 sample was prepared from $Ti(SO_4)_2$ precursor, therefore a small amount of sulfate species already existed on the surface before sulfation. After $SO_2 + O_2$ treatment, a negative band at 1363 cm^{-1} due to
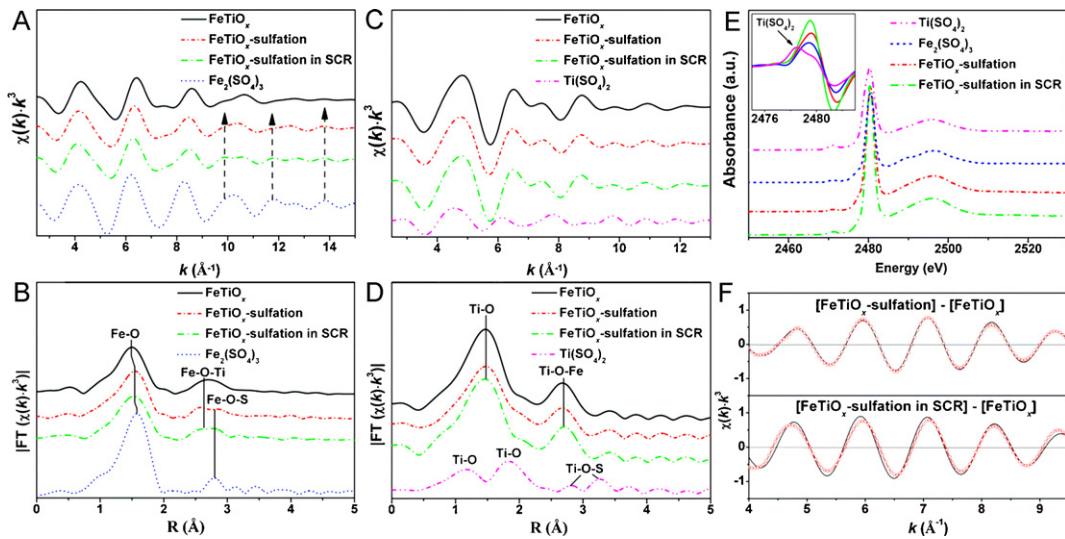
Fig. 3. XAFS results: (A) $k^3 \cdot \chi(k)$ of Fe K-edge; (B) Fourier transforms of filtered $k^3 \cdot \chi(k)$ of Fe K-edge; (C) $k^3 \cdot \chi(k)$ of Ti K-edge; (D) Fourier transforms of filtered $k^3 \cdot \chi(k)$ of Ti K-edge; (E) XANES of S K-edge and corresponding first-order derivatives (inset); (F) difference between the spectra of Fe K-edge EXAFS oscillations in FeTiO$_x$ catalysts before and after sulfation in SO$_2$ + O$_2$ and SCR condition in the R range of $ca.$ 2.3–3.1 Å (the red dots correspond to the calculated EXAFS oscillations of Fe–O–S bond in Fe$_2$(SO$_4$)$_3$ using FEFF). (For interpretation of the references to color in this figure legend, the reader is referred to the web version of the article.)

Table 2
Curve fitting results of Fe K-edge EXAFS difference spectra in FeTiO$_x$ catalysts before and after sulfation.

Samples	Bond type	Coordination number	Bond distance (Å)	DW factor (σ^2) (10^{-3} Å^2)
[FeTiO$_x$-sulfation] – [FeTiO$_x$-fresh]	Fe–O–S	1.2 ± 0.2	3.29 ± 0.01	7.6
[FeTiO$_x$-sulfation in SCR] – [FeTiO$_x$-fresh]	Fe–O–S	1.4 ± 0.1	3.28 ± 0.01	7.6

the coverage or hydration of residual sulfate species by H$_2$O was observed. Although the hydroxyl consumption bands at 3629 and 3710 cm^{-1} along with the H$_2$O adsorption band at 1614 cm^{-1} were also observed, no obvious band attributed to sulfur-containing species was found, implying the high resistance of TiO$_2$ to SO$_2$ poisoning as we mentioned above. This is in well accordance with the results from Long and Yang, in which the sulfate species could not significantly form on TiO$_2$-PILC after SO$_2$ + O$_2$ + H$_2$O treatment at 400 °C [40]. Summarizing these results we can see that, on FeTiO$_x$ catalyst the sulfation process mainly occurred on iron sites, and the SO$_2$ poisoning effect was weakened to a certain extent by the presence of titanium species in the form of Fe–O–Ti structure [16].
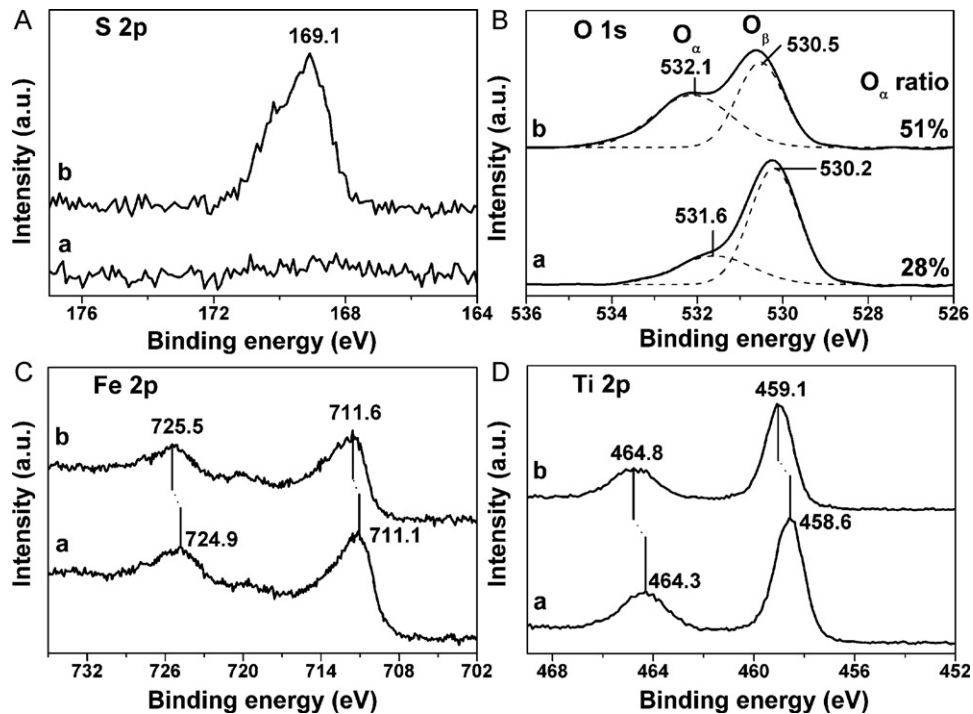
Fig. 4. XPS results of (A) S 2p, (B) O 1s, (C) Fe 2p and (D) Ti 2p in (a) FeTiO$_x$-fresh and (b) FeTiO$_x$-sulfation in SCR.
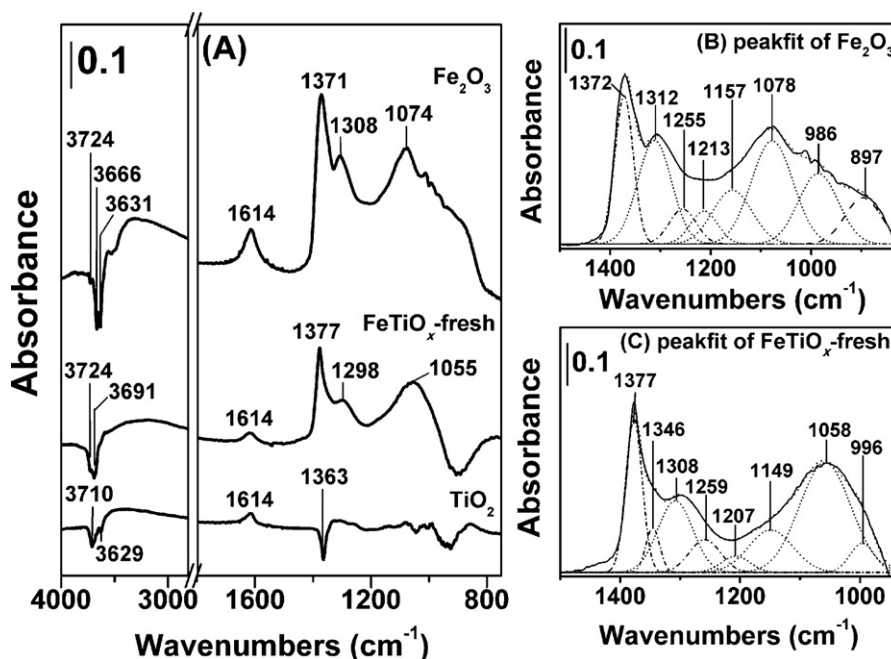
Fig. 5. *In situ* DRIFTS of $SO_2 + O_2$ treatment on Fe_2O_3, $FeTiO_x$-fresh and TiO_2 at 200 °C for 2 h and then N_2 purge for 0.5 h.

Due to the strong overlapping of bands in the range of 800–1400 cm^{-1}, it was difficult to distinguish the kinds of sulfur-containing species formed on catalyst surface. The bands were therefore deconvoluted with PeakFit software package searching for the optimal combination of Gaussian sub-bands with correlation coefficients (r^2) above 0.99, as shown in Fig. 5B and C. According to the literature, the possible sulfur-containing species may include bidentate "organic" sulfate and "inorganic" sulfate, tridentate sulfate and bisulfate [37,40–45]. For instance, on the surface of Fe_2O_3, the sub-bands at 1372 and 1255 cm^{-1} were attributed to asymmetric and symmetric stretching vibration modes of O=S=O, which were typical for "organic" sulfate species with covalent S=O double bonds [40,46]. In the presence of H_2O, partial "organic" sulfate species could transform into "inorganic" sulfate species, leading to the formation of SO_4^{2-} species with ionic S–O bonds. Therefore, the band at 1312 cm^{-1} in this case was attributed to chelating bidentate "inorganic" SO_4^{2-} bound to iron sites [40]. It has been reported that the symmetry of free SO_4^{2-} was tetragonal (T_d), giving a totally symmetric S–O stretching vibration near 980 cm^{-1} (ν_1, IR inactive) and an asymmetric triply degenerate S–O stretching vibration near 1100 cm^{-1} (ν_3, IR inactive) [42]. When the SO_4^{2-} bonded to iron sites on the sample surface in the form of chelating bidentate conformation, its symmetry was degenerated from T_d to C_{2v}, giving IR active ν_1 vibration mode together with the splitting of the ν_3 band into three bands in the range of 900–1250 cm^{-1} [42,43]. Therefore, the sub-band at 986 cm^{-1} in the spectrum of Fe_2O_3 was ascribed to the symmetric S–O stretching vibration mode of bidentate "inorganic" SO_4^{2-}, and the sub-bands at 1078, 1157 and 1213 cm^{-1} were due to its ν_3 band splits [37,41,42,44]. In addition to the bands originated from sulfate species, another band located at 897 cm^{-1} was also observed, which could be assigned to the symmetric S–O stretching vibration mode in bisulfate species (HSO_4^-, C_{3v}) [42]. As for the $FeTiO_x$ catalyst after sulfation, similar bands attributed to "organic" sulfate species ($\nu_{as\ S=O}$ at 1377 cm^{-1} and $\nu_{s\ S=O}$ at 1259 cm^{-1}) and "inorganic" SO_4^{2-} group (ν_1 at 996 cm^{-1} and ν_3 splitting bands at 1058, 1149 and 1207 cm^{-1}) were also observed, implying the formation of chelating bidentate "organic" and "inorganic" sulfates on the iron sites. Besides, another small band at 1346 cm^{-1} was also found, which could be attributed to the stretch-

ing vibration mode of the S=O double bond in tricoordinated sulfate species with three long S–O bonds and one short S=O bond standing up on the catalyst surface [45,47]. This type of sulfate species was not observed on the Fe_2O_3 surface, possibly due to the different surface structures of these two samples. Furthermore, no bisulfate species was detected on the surface of $FeTiO_x$ catalyst, which is also different from that on pristine Fe_2O_3. In summary, the sulfate species formed on $FeTiO_x$ catalyst and Fe_2O_3 sample in the sulfation process was mainly in the chelating bidentate conformation on iron sites, although a small amount of tridentate sulfate or bisulfate might also exist under certain conditions.

3.7. NH_3 and NO_x adsorption capability

The above XRD, XAFS, XPS and *in situ* DRIFTS results have shown that sulfate species was mainly formed on the iron sites of the $FeTiO_x$ catalyst after sulfation, which would lead to the enhancement of surface acidity and acid strength. This conclusion can be confirmed by the NH_3-TPD results, as shown in Fig. 6A. From the $FeTiO_x$-fresh catalyst, three NH_3 desorption peaks were detected with the increasing of temperature. As we described in previous study [48], the sharp peak at 84 °C was attributed to physisorbed NH_3, and the peak centered at 134 °C was ascribed to NH_4^+ bound to weak Brønsted acid sites (some surface hydroxyls). The broadest peak centered at 215 °C was due to the multiple desorptions of NH_4^+ bound to strong Brønsted acid sites (some surface hydroxyls with enhanced acidity induced by sulfate species and hydroxyls directly linked to sulfate species) and coordinated NH_3 bound to Lewis acid sites. After sulfation, more strong Brønsted acid sites existed on the catalyst surface, and the Lewis acid strength was also enhanced, which directly resulted in the much higher affinity of NH_3 species. Therefore, no obvious NH_3 desorption peak from $FeTiO_x$-sulfation was found below 250 °C. The *in situ* DRIFTS of NH_3 desorption from $FeTiO_x$-sulfation in Fig. S3 (Supporting Information) showed that partial NH_4^+ bound to Brønsted acid sites could transform into coordinated NH_3 bound to Lewis acid sites because of the dehydroxylation effect from 30 to 250 °C. At higher temperatures, an obvious NH_3 desorption peak centered at 354 °C was observed, which was composed of NH_4^+ bound to acidic hydroxyls
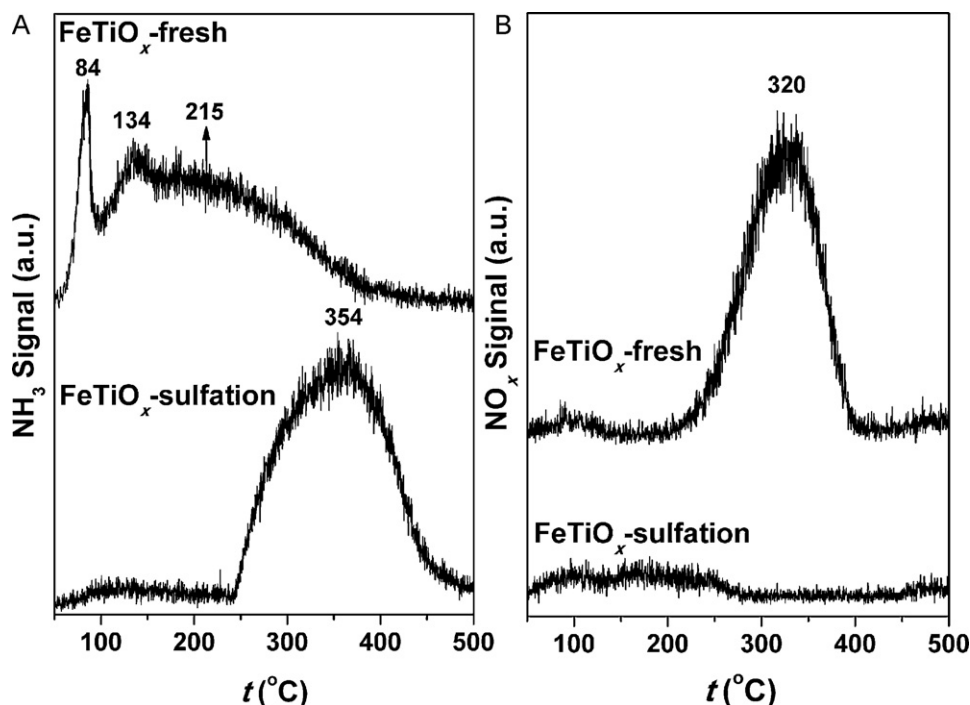
Fig. 6. (A) NH$_3$-TPD and (B) NO$_x$-TPD over FeTiO$_x$-fresh and FeTiO$_x$-sulfation.

of sulfate species and NH$_3$ bound to titanium sites with enhanced Lewis acid strength. This result implies that in the relatively high temperature range much more adsorbed NH$_3$ species could participate in the SCR reaction, leading to a shift of operation temperature window towards higher temperature range.

Our previous study already showed that the oxidation of NO to NO$_2$ and the subsequent formation of active nitrate species mainly occurred on the iron sites of FeTiO$_x$ catalyst in the low temperature SCR reaction [48]. After sulfation, the oxidation of NO to NO$_2$ (as shown in Fig. S4) and thereafter the formation of nitrate species could be strongly hindered because of the stronger acidity of sulfate species on iron sites. The comparative NO$_x$-TPD results in Fig. 6B further confirmed this point of view. From the FeTiO$_x$-fresh catalyst, a weak NO$_x$ desorption band around 100 °C together with an obvious NO$_x$ desorption band centered at 320 °C were observed. According to our previous study, the former desorption band was due to the decomposition of monodentate nitrate and the latter one to the multiple decompositions of bridging nitrate and bidentate nitrate [48]. In contrast, no obvious strong NO$_x$ desorption band was observed from FeTiO$_x$-sulfation in the whole temperature range besides of some broad and weak bands below 250 °C. Compared with the *in situ* DRIFTS of NO$_x$ desorption from FeTiO$_x$-sulfation in Fig. S3 (Supporting Information), these weak bands could be attributed to desorption of physisorbed NO and decomposition of bidentate nitrate. The NO$_x$ desorption amounts from these two samples showed that the NO$_x$ adsorption capability on FeTiO$_x$ catalyst was indeed strongly inhibited by the sulfation process. The active nitrate species could not continuously form on sulfated catalyst surface, which was disadvantageous for the low temperature SCR activity. In short summary, the inhibition of NO$_x$ adsorption capability in the relatively low temperature range and the enhancement of NH$_3$ adsorption capability in the relatively high temperature range simultaneously shifted the operation temperature window of the sulfated catalyst towards higher temperature range.

According to our previous study, the SCR reaction over FeTiO$_x$-fresh mainly followed the Langmuir–Hinshelwood (L–H)

mechanism in the low temperature range (<200 °C) and Eley–Rideal (E–R) mechanism in the high temperature range (>200 °C). Based on the TPD results above, it is deduced that only the E–R mechanism between adsorbed NH$_3$ species and gaseous or weakly adsorbed NO was present over FeTiO$_x$-sulfation, as there was almost no NO$_x$ desorbed species detected in the whole temperature range. The detailed SCR reaction mechanism over FeTiO$_x$-sulfation will be further investigated using *in situ* DRIFTS method in the following section.

3.8. Reaction mechanism over FeTiO$_x$-sulfation

The above NO$_x$-TPD results showed that there was nearly no nitrate species formed on sulfated catalyst surface, which is in well accordance with the following *in situ* DRIFTS results in Fig. 7.
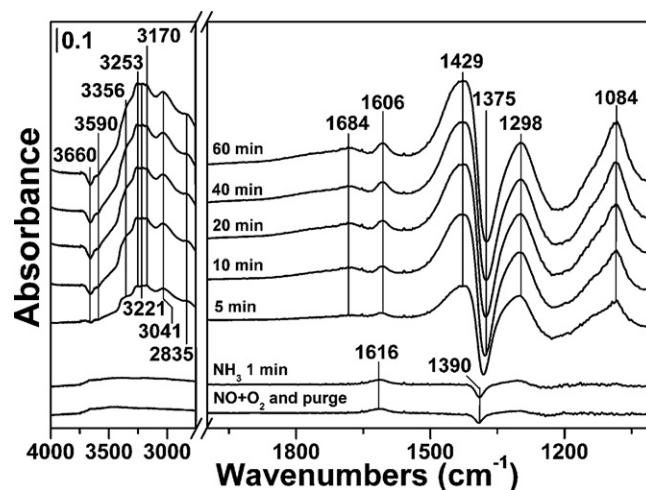

Fig. 7. *In situ* DRIFTS of reaction between NH$_3$ and pre-adsorbed NO$_x$ species at 200 °C over FeTiO$_x$-sulfation.

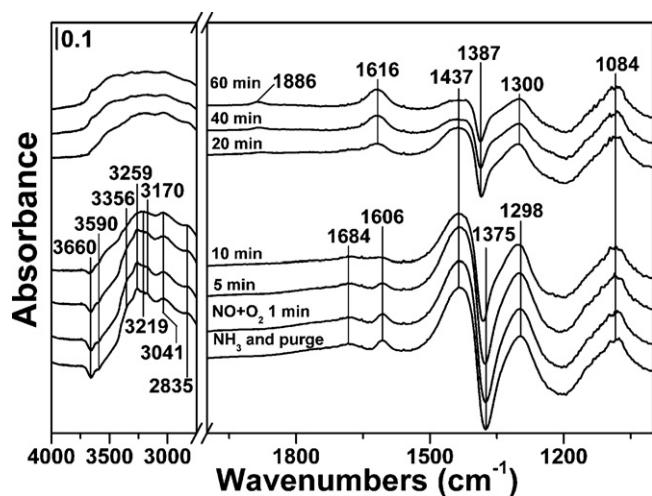**Fig. 8.** *In situ* DRIFTS of reaction between NO + O$_2$ and pre-adsorbed NH$_3$ species at 200 °C over FeTiO$_x$-sulfation.

Fig. 9. *In situ* DRIFTS of reaction in NH$_3$ + NO + O$_2$ at 200 °C over FeTiO$_x$-sulfation.

After NO + O$_2$ adsorption and N$_2$ purge at 200 °C, no infrared bands attributed to nitrate species were detected. The band at 1616 cm^{-1} was assigned to the δ_{HOH} vibration mode of adsorbed H$_2$O contained in the simulating gas, and the negative band at 1390 cm^{-1} was due to the coverage or hydration of partial residual sulfate species by H$_2$O. After the introduction of NH$_3$, strong bands attributed to adsorbed NH$_3$ species were observed, including ionic NH$_4^+$ bound to Brønsted acid sites (δ_s at 1684 cm^{-1} and δ_{as} at 1429 cm^{-1}) and coordinated NH$_3$ bound to Lewis acid sites (δ_{as} at 1606 cm^{-1} and δ_s at 1298 cm^{-1}) [40,49]. At the same time, obvious N–H stretching vibration bands from ionic NH$_4^+$ (3221, 3041 and 2835 cm^{-1}) [50–52] and coordinated NH$_3$ (3356, 3253 and 3170 cm^{-1}) [53] also appeared. Two negative bands at 3660 and 3590 cm^{-1} were caused by the consumption of surface acidic hydroxyls through the interaction with NH$_3$ to form NH$_4^+$. The intense negative band at 1375 cm^{-1} ($\nu_{as\ S=O}$) was owing to the interaction between sulfate species and NH$_3$, in which process ammonium sulfate ((NH$_4$)$_2$SO$_4$) might directly form on the catalyst surface. Therefore, it is deduced that the band at 1084 cm^{-1} was attributed to the perturbation of sulfate species ($\nu_{s\ S-O}$) through reaction with NH$_3$ to form (NH$_4$)$_2$SO$_4$. In the standard IR spectrum of (NH$_4$)$_2$SO$_4$ from NIST Chemistry WebBook, as shown in Fig. S5 in Supporting Information, a similar band at 1088 cm^{-1} was also observed, confirming the formation of surface (NH$_4$)$_2$SO$_4$ species in our case. These results imply that the catalyst surface acidity was indeed strongly enhanced by the sulfation process, and there was no occurrence of SCR reaction between adsorbed NO$_x$ species and adsorbed NH$_3$ species through L–H mechanism.

Afterwards, the *in situ* DRIFTS experiment of reaction between NO + O$_2$ and pre-adsorbed NH$_3$ species over FeTiO$_x$-sulfation was carried out and the results are shown in Fig. 8. After NH$_3$ adsorption and N$_2$ purge, the bands ascribed to ionic NH$_4^+$ (δ_s at 1684 cm^{-1} and δ_{as} at 1437 cm^{-1}) and coordinated NH$_3$ (δ_{as} at 1606 cm^{-1} and δ_s at 1298 cm^{-1}) showed up, similar to the results shown in Fig. 7. The subsequent introduction of NO + O$_2$ resulted in an evident intensity weakening of these bands, indicating the consumption of adsorbed NH$_3$ species. With the increasing of reaction time, the δ_{as} vibration band of coordinated NH$_3$ at 1606 cm^{-1} and δ_s vibration band of ionic NH$_4^+$ at 1684 cm^{-1} overlapped with the δ_{HOH} vibration band (1616 cm^{-1}) of adsorbed H$_2$O produced in the SCR reaction. The broad band in the range of 3000–3500 cm^{-1} owing to the O–H stretching vibration mode also confirmed the formation of a large amount of H$_2$O. After reaction for 60 min, the surface concentrations of both NH$_4^+$ and NH$_3$ were greatly lowered, accompanied by

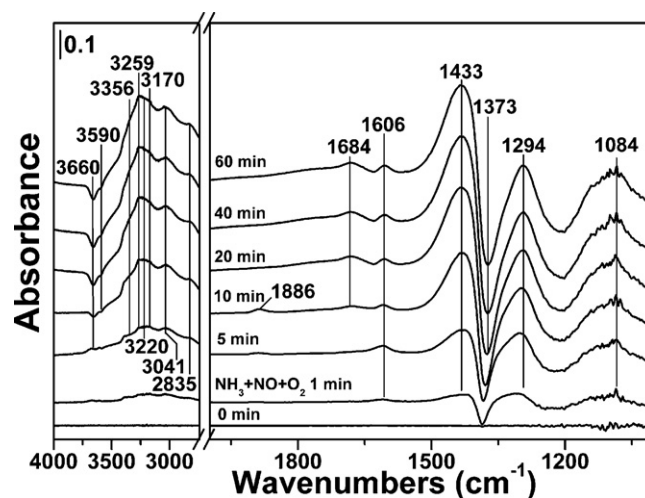the recovering of negative hydroxyl consumption bands at 3660 and 3590 cm^{-1}. The negative band at 1387 cm^{-1} was also partially recovered, which implied that the NH$_4^+$ bound to sulfate species could also take part in the SCR reaction. The small band at 1886 cm^{-1} could be attributed to the stretching vibration mode of NO in gas phase [54] when the surface reducing agent was not sufficient. During the whole reaction process, no nitrate species or other nitrogenous intermediates were found on the catalyst surface, suggesting an E–R reaction mechanism between adsorbed NH$_3$ species and gaseous or weakly adsorbed NO. The dehydrogenation of ionic NH$_4^+$ to NH$_3^+$ species [51] and coordinated NH$_3$ to NH$_2$ species [55] by adjacent Fe^{3+} may be the rate determining step, followed by subsequent reaction with NO to produce N$_2$ and H$_2$O.

Finally, the *in situ* DRIFTS experiment of SCR reaction over FeTiO$_x$-sulfation as a function of time was conducted and the results are shown in Fig. 9. During the whole SCR reaction process, only adsorbed NH$_3$ species was observed over the catalyst surface, except for a small band at 1886 cm^{-1} attributed to gaseous NO at around 10 min. This result shows again that the L–H reaction pathway was cut off due to the sulfation process and only the E–R reaction pathway dominated over this sulfated catalyst, which is in well accordance with the TPD and activity test results.

4. Conclusions

The sulfation process showed an obvious influence on the structure and SCR activity of FeTiO$_x$ catalyst. After long-time SCR reaction in SO$_2$-containing atmosphere, the surface area and pore volume showed some decrease to a certain extent, although this was not a main reason for the catalyst deactivation. According to the XRD, XAFS and XPS results, the sulfate species was mainly formed on iron sites in a chelating bidentate conformation, resulting in the higher binding energies of Fe 2p and Ti 2p due to the inductive effect of the S=O double bond. Both of the Brønsted acidity and Lewis acid strength on the catalyst surface were greatly enhanced, leading to larger NH$_3$ adsorption capability especially in the high temperature range. However, the active nitrate species could not form effectively owing to the stronger acidity of sulfate species on iron sites. Therefore, the low temperature SCR activity was inhibited due to the cutting off of the L–H reaction pathway. The operation temperature window of the sulfated catalyst shifted *ca.* 50 °C towards higher temperature range accordingly. The mechanism study shows that only the E–R reaction pathway dominated in the NH$_3$-SCR reaction over sulfated FeTiO$_x$ catalyst, which is an important reason for its enhanced SO$_2$ durability at high temperatures. For practical use,

this FeTiO$_x$ catalyst can be used for DeNO$_x$ process in SO$_2$-free conditions, or in the presence of SO$_2$ when the reaction temperature is higher than 250 °C.

Acknowledgements

Appendix A. Supplementary data

Supplementary data associated with this article can be found, in the online version, at doi:10.1016/j.apcatb.2011.01.044.

References

[1] H. Bosch, F. Janssen, Catal. Today 2 (1988) 369.
[2] G. Busca, L. Lietti, G. Ramis, F. Berti, Appl. Catal. B: Environ. 18 (1998) 1.
[3] P. Balle, B. Geiger, S. Kureti, Appl. Catal. B: Environ. 85 (2009) 109.
[4] J.P. Chen, M.C. Hausladen, R.T. Yang, J. Catal. 151 (1995) 135.
[5] C.-C. Liu, H. Teng, Appl. Catal. B: Environ. 58 (2005) 69.
[6] H. Sjövall, L. Olsson, E. Fridell, R.J. Blint, Appl. Catal. B: Environ. 64 (2006) 180.
[7] J.-H. Park, H.J. Park, J.H. Baik, I.-S. Nam, C.-H. Shin, J.-H. Lee, B.K. Cho, S.H. Oh, J. Catal. 240 (2006) 47.
[8] S.M. Jeong, S.H. Jung, K.S. Yoo, S.D. Kim, Ind. Eng. Chem. Res. 38 (1999) 2210.
[9] X. Tang, J. Hao, W. Xu, J. Li, Catal. Commun. 8 (2007) 329.
[10] Z. Wu, B. Jiang, Y. Liu, H. Wang, R. Jin, Environ. Sci. Technol. 41 (2007) 5812.
[11] G. Qi, R.T. Yang, R. Chang, Appl. Catal. B: Environ. 51 (2004) 93.
[12] M. Kang, E.D. Park, J.M. Kim, J.E. Yie, Catal. Today 111 (2006) 236.
[13] R.Q. Long, R.T. Yang, R. Chang, Chem. Commun. (2002) 452.
[14] W. Xu, H. He, Y. Yu, J. Phys. Chem. C 113 (2009) 4426.
[15] F. Liu, H. He, C. Zhang, Chem. Commun. (2008) 2043.
[16] F. Liu, H. He, C. Zhang, Z. Feng, L. Zheng, Y. Xie, T. Hu, Appl. Catal. B: Environ. 96 (2010) 408.
[17] F. Liu, K. Asakura, H. He, Y. Liu, W. Shan, X. Shi, C. Zhang, Catal. Today (2010), doi:10.1016/j.cattod.2010.10.008.
[18] Y. Cheng, C. Lambert, D.H. Kim, J.H. Kwak, S.J. Cho, C.H.F. Peden, Catal. Today 151 (2010) 266.
[19] W.S. Kijlstra, M. Biervliet, E.K. Poels, A. Bliek, Appl. Catal. B: Environ. 16 (1998) 327.
[20] F. Notoya, C. Su, E. Sasaoka, S. Nojima, Ind. Eng. Chem. Res. 40 (2001) 3732.
[21] J.W. Cook, D.E. Sayers, J. Appl. Phys. 52 (1981) 5024.
[22] A.L. Ankudinov, B. Ravel, J.J. Rehr, S.D. Conradson, Phys. Rev. B 58 (1998) 7565.
[23] P.G. Coombs, Z.A. Munir, J. Therm. Anal. Calorim. 35 (1989) 967.
[24] F. Nakajima, I. Hamada, Catal. Today 29 (1996) 109.
[25] R. Kiyoura, K. Urano, Ind. Eng. Chem. Process Des. Develop. 9 (1970) 489.
[26] Z. Zhu, H. Niu, Z. Liu, S. Liu, J. Catal. 195 (2000) 268.
[27] L.K. Boudali, A. Ghorbel, P. Grange, F. Figueras, Appl. Catal. B: Environ. 59 (2005) 105.
[28] T. Grzybek, J. Klinik, B. Buczek, Surf. Interface Anal. 23 (1995) 815.
[29] G. Xie, Z. Liu, Z. Zhu, Q. Liu, J. Ge, Z. Huang, J. Catal. 224 (2004) 42.
[30] L. Baraket, A. Ghorbel, P. Grange, Appl. Catal. B: Environ. 72 (2007) 37.
[31] M. Kang, E.D. Park, J.M. Kim, J.E. Yie, Appl. Catal. A: Gen. 327 (2007) 261.
[32] E.P. Reddy, L. Davydov, P.G. Smirniotis, J. Phys. Chem. B 106 (2002) 3394.
[33] S. Roy, B. Viswanath, M.S. Hegde, G. Madras, J. Phys. Chem. C 112 (2008) 6002.
[34] R.Q. Long, R.T. Yang, J. Catal. 207 (2002) 158.
[35] E. García-Bordejé, J.L. Pinilla, M.J. Lázaro, R. Moliner, J.L.G. Fierro, J. Catal. 233 (2005) 166.
[36] S.T. Choo, Y.G. Lee, I.-S. Nam, S.-W. Ham, J.-B. Lee, Appl. Catal. A: Gen. 200 (2000) 177.
[37] H. Fu, X. Wang, H. Wu, Y. Yin, J. Chen, J. Phys. Chem. C 111 (2007) 6077.
[38] A.L. Goodman, E.T. Bernard, V.H. Grassian, J. Phys. Chem. A 105 (2001) 6443.
[39] T.-L. Tso, E.K.C. Lee, J. Phys. Chem. 89 (1985) 1612.
[40] R.Q. Long, R.T. Yang, J. Catal. 186 (1999) 254.
[41] D. Pietrogiacomi, A. Magliano, D. Sannino, M.C. Campa, P. Ciambelli, V. Indovina, Appl. Catal. B: Environ. 60 (2005) 83.
[42] S.J. Hug, J. Colloid Interface Sci. 188 (1997) 415.
[43] Z. Zhu, Z. Liu, H. Niu, S. Liu, T. Hu, T. Liu, Y. Xie, J. Catal. 197 (2001) 6.
[44] H. Watanabe, C.D. Gutleben, J. Seto, Solid State Ionics 69 (1994) 29.
[45] E. Astorino, G. Busca, G. Ramis, R.J. Willey, Catal. Lett. 23 (1994) 353.
[46] T. Jin, T. Yamaguchi, K. Tanabe, J. Phys. Chem. 90 (1986) 4794.
[47] O. Saur, M. Bensitel, A.B.M. Saad, J.C. Lavalley, C.P. Tripp, B.A. Morrow, J. Catal. 99 (1986) 104.
[48] F. Liu, H. He, J. Phys. Chem. C 114 (2010) 16929.
[49] R.Q. Long, R.T. Yang, J. Catal. 190 (2000) 22.
[50] G. Qi, R.T. Yang, Appl. Catal. A: Gen. 287 (2005) 25.
[51] N.-Y. Topsøe, Science 265 (1994) 1217.
[52] S. Gopalakrishnan, P. Jungwirth, D.J. Tobias, H.C. Allen, J. Phys. Chem. B 109 (2005) 8861.
[53] G. Piazzesi, O. Kröcher, M. Elsener, A. Wokaun, Appl. Catal. B: Environ. 65 (2006) 55.
[54] G. Ramis, L. Yi, G. Busca, M. Turco, E. Kotur, R.J. Willey, J. Catal. 157 (1995) 523.
[55] N. Apostolescu, B. Geiger, K. Hizbullah, M.T. Jan, S. Kureti, D. Reichert, F. Schott, W. Weisweiler, Appl. Catal. B: Environ. 62 (2006) 104.